Journal of Nuclear Materials 389 (2009) 311–316

Contents lists available at ScienceDirect

Journal of Nuclear Materials

journal homepage: www.elsevier.com/locate/jnucmat

Comparison of the damage in sapphire due to implantation of boron, nitrogen, and iron

Carl J. McHargue [a,*], E. Alves [b], C. Marques [b], L.C. Ononye [c]

[a] University of Tennessee, 514 East Stadium Hall, Knoxville, TN 37996-0750, United States
[b] Instituto Tecnologico e Nuclear, Sacavém 2686-953, Portugal
[c] State University of New York – Canton, Canton, NY, United States

A B S T R A C T

The damage microstructure and optical properties of sapphire implanted with boron, nitrogen and iron were examined by RBS-C, TEM, and optical absorption. Implantations were conducted at RT and 1000 °C at 150 keV and fluences of 3×10^{16}–1×10^{17} ions/cm^2. Optical absorption measurements indicate that the boron-implanted samples contained the highest number of F-type centers and the nitrogen-implanted samples the fewest. The microstructure of the boron-implanted samples shows only 'black-spot' defect clusters, as did the iron-implanted samples at the lower fluences. At higher fluences, the iron implanted samples revealed the presence of nanometer-sized precipitates of single crystal bcc iron that contributed to additional optical scattering. Bubbles formed in samples implanted with low fluences of nitrogen. A second damage region is apparent in the RBS-C patterns for higher fluences of nitrogen.

1. Introduction

Studies of the defects produced in sapphire (single crystalline Al_2O_3) date from the in-reactor irradiations of Levy and Dienes reported in 1954 [1]. Arnold et al. subsequently demonstrated that the optical absorption band at 204 nm was due to displacements produced by energetic (50–200 keV) light ions (H^+, D^+, He^+) [2]. This absorption band has been shown to be due to F– and F^+-type centers (oxygen vacancies containing two or one trapped electrons) [3].

In subsequent years, there have been numerous studies of ion-implanted sapphire, and a general understanding of the defect structure and properties has been achieved. Nevertheless, there are details concerning the formation and retention of defects that are still unclear.

In additional to the interest in sapphire for potential applications in nuclear environments, its response to particle bombardment is of fundamental interest. While sapphire is generally classified as ionic bonded, there is a significant covalent nature in the crystal. Its crystal structure is strongly anisotropic. These factors make modeling by MD simulations difficult and there do not appear to be any such studies reported. Existing damage simulations have relied on the Monte Carlo method of TRIM and its derivatives, i.e., only ballistic displacements [4]. Sapphire exhibits essentially no deviation from stoichiometry and the solubility of impurity is below the limits of detection. The nonequilibrium introduction of implanted species requires the formation of second phases and/or defect–impurity complexes that compensate for unbalanced charges. These factors also influence the nature of the residual state of displaced Al and O ions.

The role (chemical, physical) of defects formed during irradiation and the defect structures retained after 'cool-down' are difficult to predict a priori. Biersack noted that the range (and defect) distributions calculated by TRIM change with the mass ratio of bombarding ion to target ion(s). For low mass ratios, there is a negative skewness with a tail of scattered ions extending toward the surface; whereas, for high ratios, the skewness is positive and the scattered ions extend into the target [5]. Fig. 1 contains the TRIM distributions for boron and iron implantations that illustrate this asymmetry.

This study compares the residual defect structure studied by several experimental techniques previously reported by this group as separate studies [6–11] with additional experimental observations. The ions selected for study include a light, non-gaseous element (boron), a light, gaseous element (nitrogen) and a moderately heavy cation (iron). Rutherford backscattering – ion channeling (RBS-C) is commonly used to determine the disorder in the aluminum sublattice and is often cited as a measure of 'damage'. Optical absorption is sensitive to oxygen vacancies with trapped electrons and may also exhibit scattering from nanometer-sized second phases. Electron microscopy provides details about the microstructure on the nanometer scale. The studies reported here employed all three techniques.

* Corresponding author. Tel.: +1 865 974 7680; fax: +1 865 974 4995.
E-mail address: crl@utk.edu (C.J. McHargue).

0022-3115/$ - see front matter © 2009 Elsevier B.V. All rights reserved.
doi:10.1016/j.jnucmat.2009.02.025

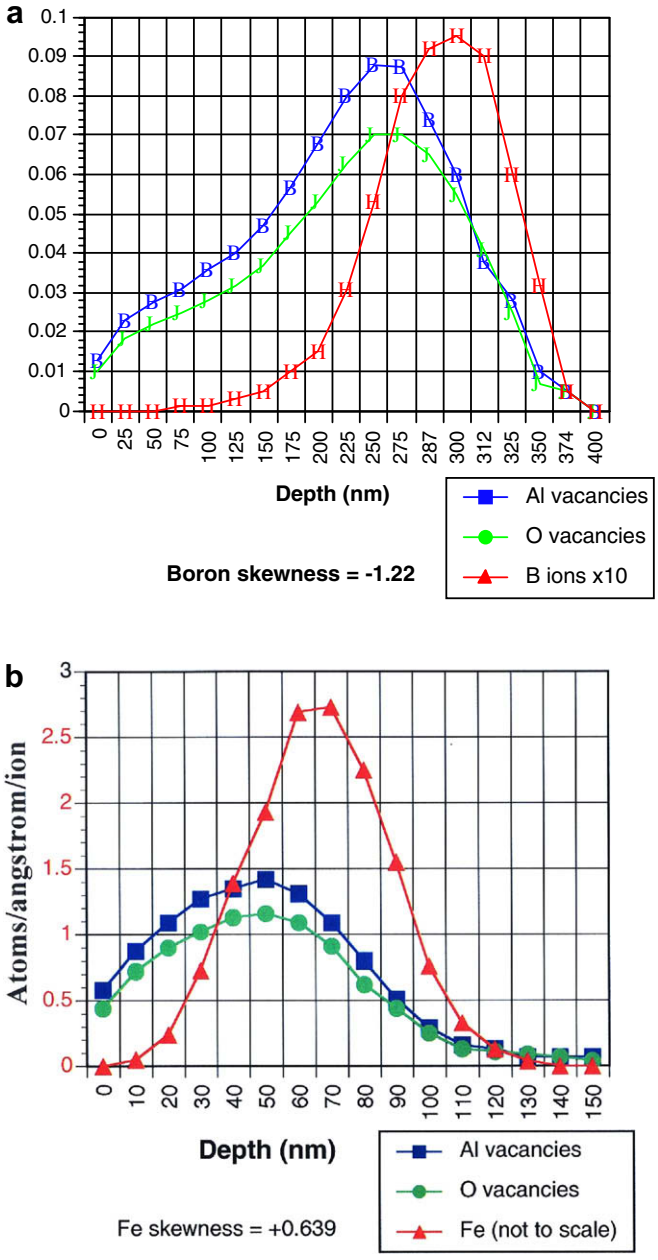

Fig. 1. TRIM calculated range and vacancy distributions for (a) boron and (b) iron implanted into sapphire at 150 keV.

2. Experimental details

High purity single crystals of α-Al_2O_3 (Crystal Systems, Inc., Bedford, MA) with optically polished surfaces parallel to {0001} planes were annealed at 1500 °C in flowing oxygen to remove any surface damage due to processing. Samples were implanted at 150 keV with 1×10^{17} B/cm^2 (RT, 500, 1000 °C), 3 and 10×10^{16} N/cm^2 (RT, 1000 °C) and $2–10 \times 10^{16}$ Fe/cm^2 (RT, 1000 °C). The beam was tilted 7° from the *c*-axis to prevent channeling. RBS-C measurements were performed with 2.0 or 2.65 MeV He^+ beams and silicon barrier detectors placed at 140° and 180° in the standard IBM geometry. Optical absorption measurements were made with a Varian Cary 5G IR–VIS–UV spectrometer. Cross-sectional TEM specimens were prepared by mechanical polishing and focused ion beam (FIB) thinning. The specimens were examined at 200 kV with HF-2000 and HD-2000 STEM.

3. Results

3.1. Boron implantation

The RBS-C spectra from the *c*-axis direction of samples show that the un-implanted crystals contain very little disorder, Fig. 2. The spectra taken with the <0001> axis aligned with the He^+ beam for the sample implanted at room temperature show increasing de-channeling from a depth of about 50 nm to almost random values at depths of 200–300 nm, Fig. 2. The spectra taken with other crystallographic directions aligned with the He^+ beam exhibited similar de-channeling effects suggesting a random distribution of the disorder in the Al-sublatice (or defects oriented parallel to the surface). The projected range (R_p) and straggling (ΔR_p) for 150 keV B is about 360 nm. The almost random values appear to lie in the region of maximum Al and O displacements, i.e., vacancies produced. Such high values of de-channeling could indicate the presence of a buried amorphous layer or a high density of defects without the complete loss of crystallinity.

The cross-sectional TEM photographs and SAD electron diffraction patterns of the RT-implanted samples (e.g., Fig. 3) contain no indication of an amorphous structure in the implanted region, but a rather uniform distribution of unidentified 'black-spot' defects. The 'damage' or implanted-induced defect structure extends to about 400 nm or equal to about $R_p + 2\Delta R_p$ (ca. 420 nm) as calculated using SRIM 2004. There is no indication of damage beyond the end of the boron distribution, although there is the suggestion of a higher density of defects at the end-of-range. The simulations indicate the presence of relatively few knock-ons beyond the range of the implanted boron ions.

The electron microscopy examination shows a rather uniform distribution of an unidentified defect throughout the implanted regions with some greater amounts near the end-of-range. In contrast, the RBS-C spectra indicate little de-channeling from the Al-sublattice in the region from the surface to a depth of about 50 nm.

The optical absorption at wavelengths near 200 nm in the RT-implanted sample, Fig. 4, is very high. This peak has been ascribed to F– and/or F^+-centers [3]. There is a second distinct peak near 270 nm that may be from F^+-centers, although it could be caused by scattering from clusters of defects or Mie scattering from nanometer-sized particles. There is a small peak near 355 nm that has been ascribed to F_2^+ clusters [3]. These optical data suggest a high concentration of oxygen vacancies that contain one or two trapped electrons. These observations are consistent with those of Agnew who used optical absorption measurements to study the damage efficiency, defined as the ratio of defects retained compared to the calculated number produced [12]. He found the number of F-centers retained in B-implanted sapphire to be significantly higher than for implantation of H, D, He, N, Ne, Ar, or Kr.

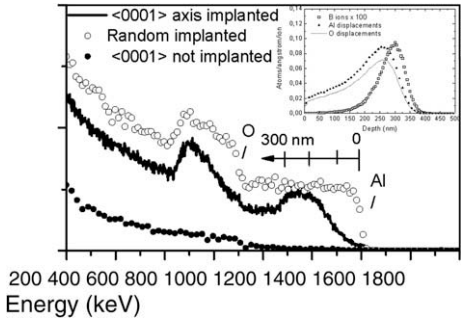

Fig. 2. Random and *c*-axis aligned RBS-C spectra obtained with 2.65 MeV He^+ for sample implanted with 1×10^{17} B/cm^2 (150 keV) at room temperature.

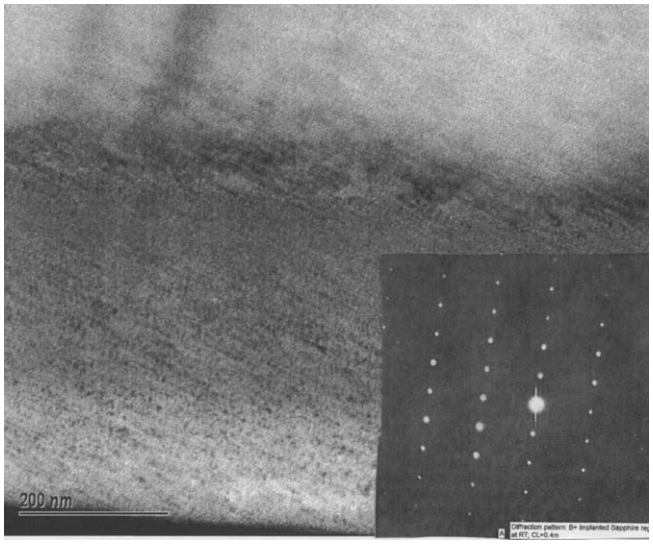

Fig. 3. Cross-sectional TEM and SAD photograph for sample implanted with 1×10^{17} B/cm^2 at room temperature.

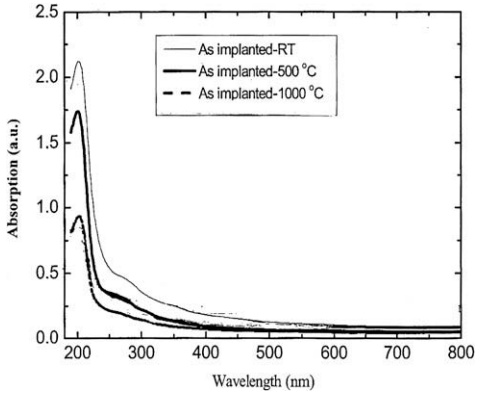

Fig. 4. Optical absorption of sapphire implanted with boron as indicated.

RT-implanted samples were annealed for 1 h at 1000 °C in a reducing atmosphere (Ar/4% H). The optical absorption was reduced to values similar to those obtained for samples implanted at 1000 °C shown in Fig. 4. The electron micrographs contained slightly fewer defect clusters [11]. The defect structure, thus, appears to be very stable.

De-channeling in the RBS-C spectra for the sample implanted at 1000 °C is less than for the RT sample at all depths, Fig. 5. However, significant de-channeling is observed at depths of 250–350 nm from the surface. This is the region of very high de-channeling in the RT-implanted samples.

The TEM micrograph (not shown) contains fewer defect clusters than the RT-implanted sample. The damage region of those micrographs extends to 500 nm indicating some in-diffusion of the defects or implanted boron. There is no evidence for a second phase and the SAD pattern is similar to Fig. 3.

The optical absorption in the range 200–400 nm is less than the RT samples, indicating fewer F-type centers and, thus, oxygen vacancies, Fig. 4. The intensity of the peak at 270 nm is also much reduced. The intensity of the peak near 200 nm is rather high, comparable to that for 1×10^{17} Fe/cm^2 implanted at the same temperature. A sample implanted at 500 °C exhibited only slightly lower optical absorption than RT-implanted samples over the range of wavelengths measured.

The amount of retained damage is surprisingly high, particularly for the RT implantation, when compared to that produced by implantation of heavier cations to higher amounts of deposited damage energy. De-channeling in the RBS-C spectra appears to originate from the 'black-spot' damage, thought to be interstitial clusters. The damage peak observed in the channeling spectrum from the 1000 °C sample is near to the depth of SRIM-predicted B range (R_p). This together with the high de-channeling observed in the same region for the RT-implanted samples suggests that some interaction between the boron and defects may occur and stabilizes some particular type of defect structure. Simulation using SRIM predicts about three times as many aluminum ions as oxygen ions are displaced due the large difference in displacement energies. The excess of aluminum displaced ions could lead to formation of aluminum interstitial clusters. Some 'black-spot' damage may be interstitial clusters of Al_2O_3. This could explain the thermal stability of damage during implantation or annealing at high temperatures.

3.2. Nitrogen implantation

It is commonly assumed that gases are inert when implanted into sapphire. It has been reported that high fluences can produce blistering and exfoliation of the surface [13,14]. Hioki et al. noted that implantation of nitrogen into sapphire resulted in blisters and nitrogen loss for fluences greater than 2×10^{17} N/cm^2 [15]. Soumoy et al. detected a buried amorphous layer in samples implanted with 7×10^{15} N/cm^2 (50 keV) at 25 °C [16].

The RBS-C spectra of Fig. 6 show the evolution of disorder with increasing nitrogen ion fluence at RT. Disorder (de-channeling) is low from the surface to a depth of ~75 nm. The de-channeling increases to a peak at about 250 nm in the sample implanted with 3×10^{16} N/cm^2. Calculations using the SRIM 2003 code give the range for 150 keV nitrogen ions of 247 nm with a straggling of

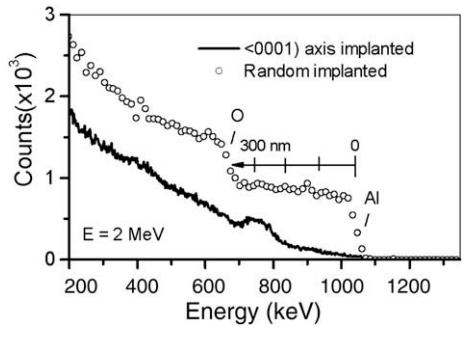

Fig. 5. Random and *c*-axis aligned RBS-C spectra obtained with 2.0 MeV He$^+$ for sapphire implanted with 1×10^{17} B/cm^2 (150 keV) at 1000 °C.

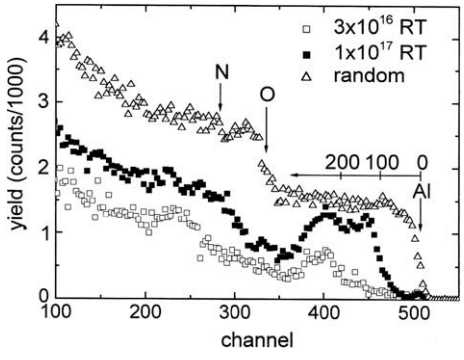

Fig. 6. Random and *c*-axis aligned RBS-C spectra for samples implanted with 3×10^{16} and 1×10^{17} N/cm^2 (150 keV) at room temperature.

57 nm. The observed de-channeling range closely corresponds to the calculated nitrogen distribution.

The dark field TEM photograph of Fig. 7 clearly shows the presence of a band of bubbles in the region of 100– 300 nm from the surface. These features are in the size range of 1–10 nm, although there may be smaller ones not imaged. The TEM examinations did not detect other defects for 3×10^{16} N/cm^2.

The RBS-C spectra and the TEM examination suggests that the formation of nitrogen bubbles displace Al ions from normal lattice sites which leads to de-channeling in the Al spectrum.

For the lower fluence, the optical absorption spectra of the RT- and 1000 °C-implanted samples (Fig. 8) are indistinguishable and the absorption is much lower than for the B-implanted sample shown in Fig. 4. The data suggest a low residual concentration of oxygen vacancies containing trapped electrons.

A second de-channeling feature is present in the spectra of samples implanted to the higher fluence of 1×10^{17} N/cm^2. This defect band lies closer to the surface and is centered at about 150 nm. The displacement profiles calculated using SRIM03 show the Al and O recoils lie closer to the surface than the implanted nitrogen (similar to the profile for boron shown in Fig. 1). This damage region then may be due to interstitial clusters of Al or Al_2O_3.

For samples implanted with nitrogen at 1000 °C, the de-channeling in the Al-sublattice is higher than in the RT-implanted samples at all depths greater than ~25 nm from the surface. Fig. 9. The de-channeling (X_{Al}) reaches a value of ~0.45 at 230 nm, close to the calculated R_p for 150 keV nitrogen.

The cross-section electron micrograph of Fig. 10 confirms the presence of many more defects than in the RT samples. There appear to be both bubbles (or voids) and point defect clusters. Some of the defects exhibit a planar character.

The optical absorption spectrum of the 1000 °C sample was indistinguishable from that for the lower fluence sample; hence, the defects produced at 1000 °C have relatively little effect on the F-type center concentration.

3.3. Iron implantation

Our earlier study that used conversion electron Mössbauer spectroscopy, RBS-C, and TEM detected the presence of metallic iron (Fe^0) in sapphire implanted with fluences of 2×10^{16} Fe/cm^2 and higher [7]. The relative amount of metallic iron increased from ~5% at 2×10^{16} Fe/cm^2 to ~36% at 1×10^{17} Fe/cm^2. As shown in

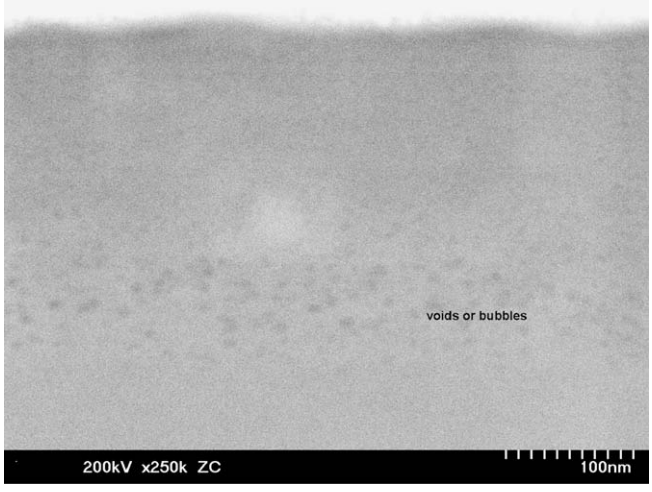

Fig. 7. Cross-sectional dark field TEM photograph of sapphire implanted with 3×10^{16} N/cm^2 at room temperature. Note the band of 'bubbles' lying 100–300 nm from surface.

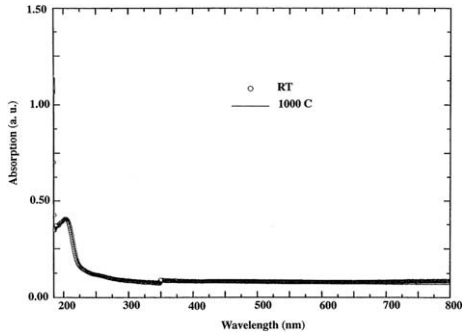

Fig. 8. Optical absorption of sapphire implanted with nitrogen (fluence = 3×10^{16} N/cm^2).

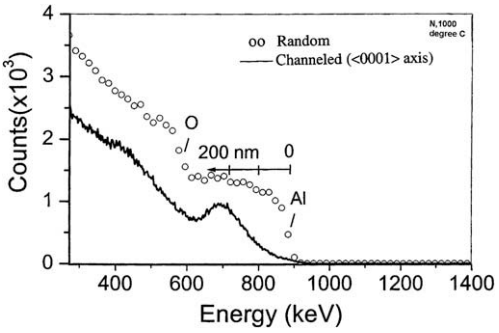

Fig. 9. Random and *c*-axis aligned RBS-C spectra for samples implanted with 3×10^{16} N/cm^2 (150 keV) at 1000 °C.

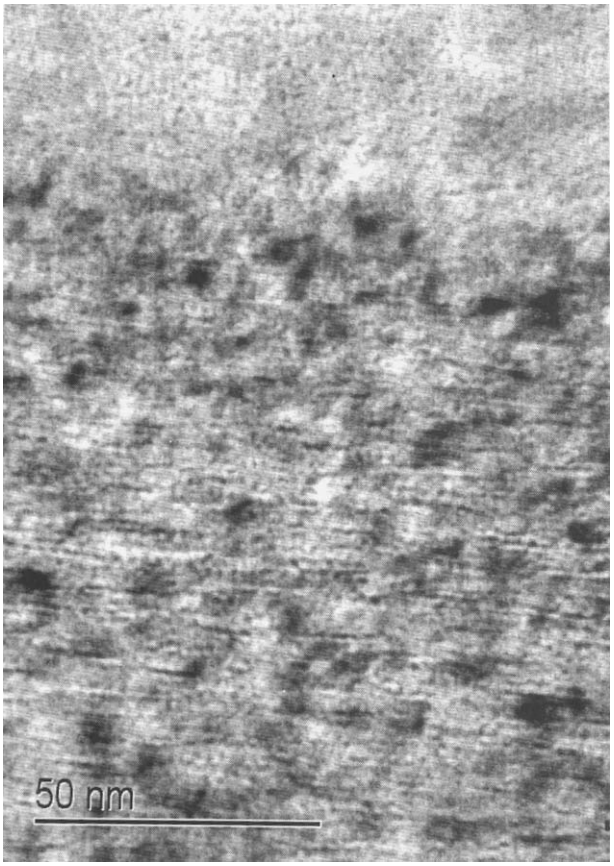

Fig. 10. Cross-sectional TEM photograph of sapphire implanted with 3×10^{16} N/cm^2 at 1000 °C.

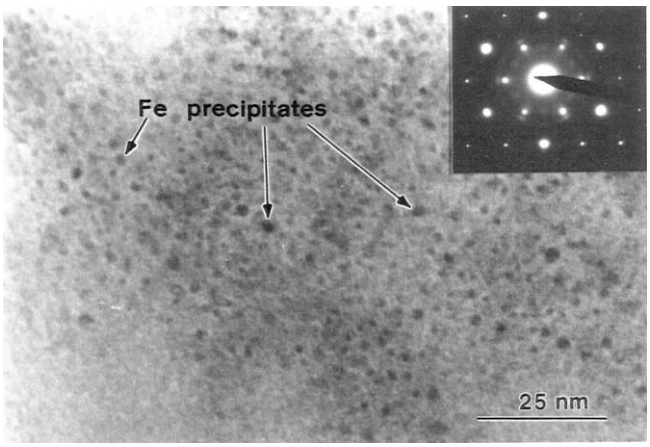

Fig. 11. Cross-sectional TEM and SAD photograph for sapphire implanted with 1×10^{17} Fe/cm^2 at room temperature. The precipitates are single crystalline body-centered cubic iron.

Fig. 11, SAD confirmed that the sample implanted with 1×10^{17} Fe/cm^2 contained 1–3 nm particles that are single crystalline α-Fe. The rest of the iron was present in the 2+ state for fluences below 5×10^{16} Fe/cm^2. At higher fluences, the iron was distributed between the metallic state and the 2+ and 4+ states. The latter charge state has been attributed to covalent Fe(IV)–O bonds wherein the Fe(IV) resides in highly distorted octahedral sites with the presence of large concentrations of oxygen vacancies [17].

The microstructure (TEM) for samples implanted with 1–4×10^{16} Fe/cm^2 is characterized by a tangled dislocation array extending to approximately the depth of maximum energy deposition [7]. Most of the network dislocations lie in the basal plane.

The RBS-C spectra indicate increasing de-channeling in the Al-sublattice with increasing fluence, reaching a maximum of $\chi_{Al} \sim 0.67$ at 145 nm for 1×10^{17} Fe/cm^2, Fig. 12. This disorder extends well beyond the position of peak displacement energy deposition (35 nm) or the range plus straggling (89 nm) for 150 keV iron. This observation is consistent with the often reported occurrence of damage that extends to 2–3 time the 'end-of-range'. The iron spectra for aligned and random are coincident, indicating the iron to be incoherent with the matrix.

The optical absorption for samples implanted with iron at RT is shown in Fig. 13. The peak near 200 nm increases with increased fluence, but is significantly lower than that for boron-implanted samples. The broad band in the region of 250–400 nm may be arise from Mie scattering from the metallic precipitates. Luminescence measurements on these samples confirmed the presence of both F– and F$^+$-centers [18].

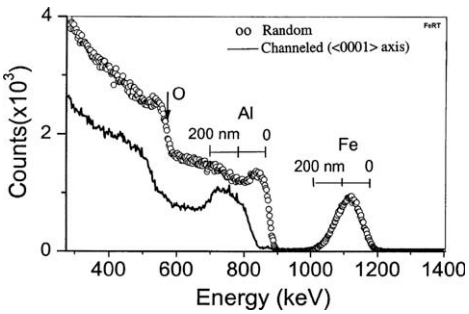

Fig. 12. Random and *c*-axis aligned RBS-C spectra for samples implanted with 1×10^{17} Fe/cm^2 (150 keV) at room temperature.

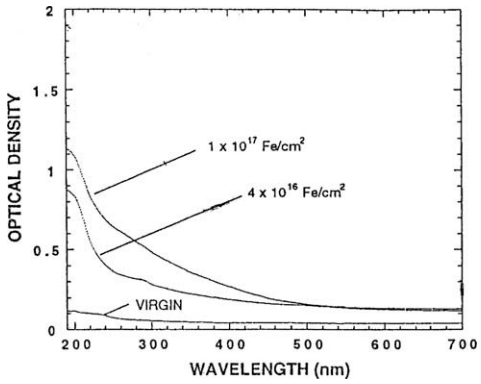

Fig. 13. Optical absorption of sapphire implanted with iron.

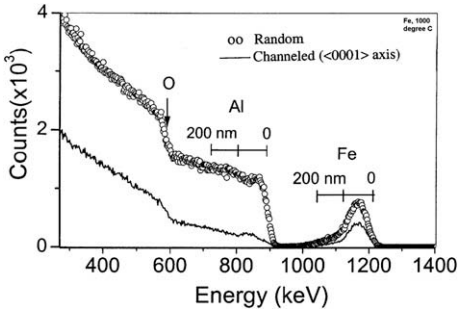

Fig. 14. Random and *c*-axis aligned RBS-C spectra for samples implanted with 1×10^{17} Fe/cm^2 (150 keV) at. 1000 °C.

The RBS-C spectra of Fig. 14 indicate very little residual disorder in the Al-sublattice in samples implanted at 1000 °C. The iron peak is asymmetrical with a tail extending into the crystal, indicating that iron has diffused from the implanted region into the sample. Only about 90% of the implanted fluence has been retained in the sample.

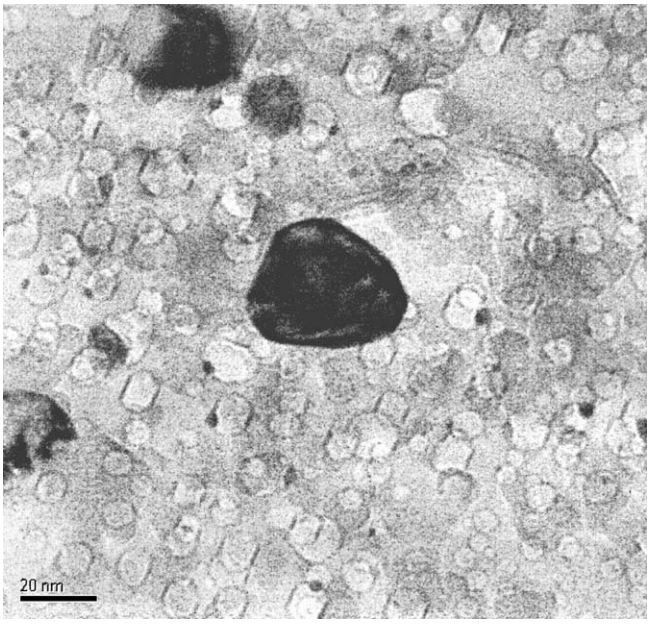

Fig. 15. Cross-sectional TEM photograph for sample implanted with 1×10^{17} Fe/cm^2 at 1000 °C. The particles are iron precipitates and are associated with voids.

The cross-section TEM of Fig. 15 shows the presence of two size distributions of second phase particles: 1–3 and 30–50 nm. X-ray diffraction and SAD identified these particles as α-Fe. Many of the particles are faceted and most are associated with a void or bubble. We have proposed that the Fe in the 2+ state is accompanied by oxygen vacancies according to the model of Catlow et al. [19] for charge compensation, and that the complex migrates as a unit. When the iron precipitates as a metal the associated vacancies precipitate as voids.

4. Summary

Implantation of boron, nitrogen and iron at room temperature and at 1000 °C produce distinctly different microstructures. Samples implanted with boron contain a very high concentration of F-type centers even in the absence of dense damage structures imaged by transmission electron microscopy. Implanted nitrogen collects into bubbles at a fluence of 3×10^{16} N/cm^2 and appears as bubbles plus an additional defect zone at 1×10^{17} N/cm^2. Optical absorption measurements indicate the presence of relatively few F-type centers. At low fluences, implanted iron is present as Fe^{2+}, accompanied by oxygen vacancies and a tangled dislocation structure. At higher fluences, much of the iron precipitates as metallic, single crystalline α-Fe and the balance is in the 2+ or 4+ state, probably accompanied by oxygen vacancies.

The de-channeling in RBS-C spectra arises from different microstructural features in these three instances, indicating the need to use multiple characterization techniques in studying implantation effects.

References

[1] P.W. Levy, G.J. Dienes, Report of Bristol Conference on Defects in Crystalline Solids, The Physical Society, London, 1955, p. 256.
[2] G.W. Arnold, G.B. Krefft, C.B. Norris, Appl. Phys. Lett. 25 (1974) 540.
[3] Y. Chen, M.M. Abraham, D.F. Pedraza, Nucl. Instrum. Meth. B 59&60 (1991) 1163.
[4] J.F. Ziegler, J.P. Biersack, U. Littmark, Stopping Power and Ranges of Ions in Matter, Pergamon, New York, 1985.
[5] J.P. Biersack, in: P. Mazzoldi, G.W. Arnold, (Eds.), Ion Beam Modification of Insulators, Elsevier, Amsterdam, 1987, p. 39.
[6] Carl J. McHargue, S.X. Ren, L.F. Allard, Y. Chen, J. Hunn, R.K. Williams, A. Perez, G. Marest, NanoStruct. Mater. 6 (1995) 513.
[7] Carl J. McHargue, P.S. Sklad, C.W. White, G.C. Farlow, A. Perez, G. Marest, J. Mater. Res. 6 (1991) 2146.
[8] Carl J. McHargue, L.C. Ononye, E. Alves, C. Marques, L.F. Allard, Nucl. Instrum. Meth. B 218 (2004) 227.
[9] E. Alves, C. Marques, L.C. Ononye, C.J. McHargue, Nucl. Instrum. Meth. B 218 (2004) 222.
[10] Carl J. McHargue, L.C. Ononye, L.F. Allard, E. Alves, M.F. DaSilva, J.C. Soares, Nucl. Instrum. Meth. B 191 (2002) 629.
[11] Carl J. McHargue, E. Alves, L.C. Ononye, C. Marques, Nucl. Instrum. Meth. B 250 (2006) 81.
[12] P. Agnew, Nucl. Instrum. Meth. B 65 (1992) 305.
[13] G.C. Farlow, C.W. White, C.J. McHargue, B.R. Appleton, Radiat. Eff. 97 (1986) 257.
[14] Carl J. McHargue, G.C. Farlow, M.B. Lewis, J.M. Williams, Nucl. Instrum. Meth. B 19&20 (1987) 809.
[15] T. Hioki, A. Itoh, S. Noda, H. Doi, J. Kawamoto, O. Kamigaito, Nucl. Instrum. Meth. B 7&8 (1985) 521.
[16] C. Soumoy, F. Bodart, J. Chevallier, Nucl. Instrum. Meth. B 85 (1994) 516.
[17] J.A. Sawicki, G. Marest, B. Cox, in: C.J. McHargue, R. Kossowsky, W.O. Hofer, (Eds.), Structure Property Relationships in Surface-Modified Ceramics, Kluwer, Dordrecht, 1989, p. 209.
[18] S.X. Ren, C.J. McHargue, L.F. Allard, Y. Chen, J.D. Hunn, B.N. Lucas, R.K. Williams, MRS Proceedings 373 (1995) 305.
[19] C.R.A. Catlow, R. James, W.C. Mackrodt, R.F. Stewart, Phys. Rev. B 25 (1982) 1006.